Journal of Alloys and Compounds 509 (2011) 8082–8087

Contents lists available at ScienceDirect

Journal of Alloys and Compounds

journal homepage: www.elsevier.com/locate/jallcom

Reddish orange long afterglow phosphor $Ca_2SnO_4:Sm^{3+}$ prepared by sol–gel method

Zheng-Hua Ju[a], Shui-He Zhang[b], Xiu-Ping Gao[a,b], Xiao-Liang Tang[a], Wei-Sheng Liu[a,*]

[a] Key Laboratory of Nonferrous Metals Chemistry and Resources Utilization of Gansu Province and State Key Laboratory of Applied Organic Chemistry, College of Chemistry and Chemical Engineering, Lanzhou University, Tianshui south road 222, Lanzhou 730000, PR China
[b] School of Physical Science and Technology, Lanzhou University, Lanzhou 730000, PR China

ARTICLE INFO

Article history:
Received 6 December 2010
Received in revised form 10 May 2011
Accepted 13 May 2011
Available online 19 May 2011

Keywords:
Reddish orange emissive
Long afterglow
$Ca_2SnO_4:Sm^{3+}$
Sol–gel
Thermoluminescence
Phosphorescence mechanism

ABSTRACT

A reddish orange light emissive long afterglow phosphor, $Ca_2SnO_4:Sm^{3+}$ was prepared by sol–gel method at lower temperature. The synthesized phosphors were characterized by X-ray diffraction, scanning electron micrograph images, photoluminescence spectra, afterglow decay curves and thermoluminescence spectra. Three emission peaks locate at 565 nm, 609 nm and 655 nm corresponding to CIE chromaticity coordinates of $x = 0.53$ and $y = 0.47$, which indicates the reddish orange light emitting. The fluorescent intensity and the afterglow characteristic depends on the concentration of Sm^{3+} and the optimized concentration is 1.5 mol%. The afterglow decay curves are well fitted with triple-exponential decay models. The thermoluminescence glow curves show that the Sm^{3+} induces suitable trap depth and result in the long afterglow phenomenon, and the corresponding increase or decrease in afterglow is associated with trap concentration, nearly no change in trap depth. The 1.5 mol% Sm^{3+}-doped Ca_2SnO_4 sample has the biggest trap concentration and exhibit the best afterglow characteristic, its' afterglow time is about 1 h. The phosphorescence mechanism of this long afterglow phosphor was discussed.

1. Introduction

Long afterglow phosphors (LAPs) is a kind of energy-storing material which can absorb energy and then gradually emit visible light for a long time after the excitation is turned off [1]. These materials are used for lighting, display, detection of high energy rays, multidimensional optical memory and imaging storage [2–6], even to supply light to solar cells in complete darkness [7]. The yellow-green, green-blue, green and blue LAP with high brightness and long persist time have been available in the commercial market [2,8–11]. However, afterglow properties of orange to red LAP is still far away from expected target [12]. The red LAP with better luminescent property is difficult to achieve, and there is still lack of orange to red long afterglow phosphors [13–15]. Although much effort has been devoted to the research of orange to red long afterglow materials, but the progresses is very slow [16]. Hence, there is a great demand to develop orange to red LAP, and it has been a focus in this field.

It is well known that the solid-state reaction process is a conventional method for phosphor synthesis, and it requires high calcinations' temperature. In recent years, numerous methods have been employed to prepare phosphors, including sol–gel process [17–19], chemical precipitation method [20,21], combustion synthesis [22,23], combustion-assisted synthesis method [24,25], sol–gel-combustion process [16], microwave-assisted-sol–gel route [26], reverse microemulsion method [27,28], hydrothermal method [29,30], spray pyrolysis method [31,32], template assisted co-deposition method [33], etc. Among them, sol–gel process is an efficient technique for the preparation of phosphors; it has some advantages, such as good mixing of starting materials, relatively low reaction temperature and more homogeneous products [34,35].

In this study, we report a reddish orange afterglow phosphor $Ca_2SnO_4:Sm^{3+}$ prepared by sol–gel method at lower temperature. Ca_2SnO_4 can be prepared by solid-state reaction at temperature of 1250–1300 °C [36]. In rare-earth ions, Sm^{3+} is an important activator for many different inorganic lattices producing reddish orange light emitting due to its $^4G_{5/2} \rightarrow {}^6H_J$ ($J = 5/2$, 7/2, 9/2, 11/2) transitions [31,37,38]. For example, Lakshminarayana et al. reported photoluminescence properties of Sm^{3+}, Dy^{3+} and Tm^{3+}-doped transparent oxyfluoride silicate glass ceramics containing CaF_2 nanocrystal [39]. These glass ceramics have potential technological applications in optoelectronic materials and displays. White light emission from Sm^{3+}/Tb^{3+} co-doped oxyfluoride aluminosilicate glasses under UV light excitation was also reported by Lakshminarayana et al. [40]. The glasses are promising for white LED. The Sm^{3+} ion was adopted as activator for present material to create long-lasting phosphorescence. The surface morphology,

* Corresponding author. Tel.: +86 931 8915151; fax: +86 931 8912582.
E-mail address: liuws@lzu.edu.cn (W.-S. Liu).

0925-8388/$ – see front matter © 2011 Elsevier B.V. All rights reserved.
doi:10.1016/j.jallcom.2011.05.050

photoluminescence (PL) and afterglow characteristics were studied. Since thermoluminescence (TL) technique is a very useful tool to reveal valuable information about the traps and their role in determining the spectroscopic properties of long persistent phosphor [41–45], the thermoluminscent spectra of the phosphors were studied, indicating there appears suitable trap depth which results in long-lasting phosphorescence. In addition, the phosphorescence mechanism of this long afterglow phosphor was discussed.

2. Experimental

2.1. Samples preparation

In solid state reaction, the powder sample $Ca_2SnO_4:Sm^{3+}$ was using $CaCO_3$ (A.R.), SnO_2 (A.R.) and Sm_2O_3 (99.99%) as raw material, NH_4Cl (A.R.) and H_3BO_3 (A.R.) as flux. Appropriate amount of raw material and flux were thoroughly mixed in an agate mortar and then triturated with distilled ethanol for an ideal mixing. Afterwards, the mixtures were put into an alumina crucible and calcined in a muffle furnace at 1250–1300 °C for 4 h in air, followed by subsequent cooling in air to ambient temperature.

In sol–gel preparation, the starting materials were $Ca(NO_3)_2{\cdot}4H_2O$ (AR), $SnCl_4{\cdot}5H_2O$ (AR), Sm_2O_3 (99.99%), HNO_3 (AR) and citric acid ($C_6H_8O_7{\cdot}H_2O$, AR). Sm^{3+} was introduced in the form of $Sm(NO_3)_3$ by dissolving Sm_2O_3 in dilute HNO_3 solution. A typical process is described as follow: 30 mmol citric acid was added to a 100 mL of aqueous solution containing 10 mmol $SnCl_4{\cdot}5H_2O$, 0.10 mmol samarium nitrate and 29.9 mmol $Ca(NO_3)_2{\cdot}4H_2O$ stirred for 3 h. Afterwards, the solutions were keeping at 90 °C under constant stirring and became viscous. The sol was continue dried at 90 °C and obtained dried gels. The dried gels were heated for 2 h on an electric stove, and then were ground. The gels were put into alumina crucibles and calcined in a muffle furnace at 900 °C for 6 h in air, followed by subsequent cooling in air at ambient temperature to obtain the final products. The obtained samples were ground lightly into powders and taken to characterization. The samples with content of Sm^{3+} at 0.5 mol%, 1.0 mol%, 1.5 mol%, 2.0 mol% were labeled as S_1, S_2, S_3 and S_4, respectively.

2.2. Measurements

The thermogravimetry-differential scanning calorimetry (TG-DSC) curves of the dried gels (19.8780 mg) for $Ca_2SnO_4:Sm^{3+}$ precursor was measured at 26–1000 °C by a Mettler Toledo TGA/DSC1 thermogravimetric analyzer in air atmosphere, the gels was heated at a rate of 10 °C min^{-1}. The synthesized products were characterized by X-ray diffraction (XRD) using a RigakuD/MAX-2400 X-ray diffractometer over the range of 10–90°, operating at 40 kV and 60 mA, with a step of 0.02° using CuKαX-rays of wavelength 1.5406 Å. Scanning electron micrograph (SEM) images were taken with a JEOL JSM-6380LV scanning electron microscopy.

The photoluminescence (PL) spectra were measured by a Hitachi F-4500 fluorescence spectrophotometer equipped with a xenon lamp as the excitation source. The excitation spectra were obtained scanning from 320 to 575 nm monitored at 609 nm. The emission spectra were scanned from 580 to 630 nm while excited at 409 nm. Both slit widths of 5 nm at the excitation and emission side. The chromaticity coordinates have been calculated from the spectra using the CIE (Commission International de l'Eclairage, France) system.

The afterglow decay properties measurement were performed on a long afterglow phosphor photometer PR305 (Zhejiang University Sensing Instruments Co., Ltd., China) with 1000Lx xenon lamp as excitation source. Minimum resolution is 10^{-2} mcd/m^2. For the afterglow spectra measurement, phosphors were firstly irradiated with 1000Lx D65 lamp for 10 min, then a FMS-I fluorescent spectroradiometer was employed to record emitting brightness after D65 lamp was turned off for 1 s. The afterglow time measurements also use 1000 Lx xenon lamp as excitation source.

The thermoluminescence (TL) spectra measurements were performed by heating the irradiated sample from 303 to 553 K using the FJ-427A1 TL meter (Beijing Nuclear Instrument Factory, China). The sample (2.0 mg) was first excited for 15 min using 254 nm UV radiation standard lamp with a power of 9 W. Then the radiation source was removed and the sample was heated at a linear rate of 1 K/s.

All measurements were carried out at room temperature except for the TG-DSC curves and TL spectra.

3. Results and discussion

The TG-DTA curves of dried gels for $Ca_2SnO_4:Sm^{3+}$ precursor are shown in Fig. 1. It can be seen that the dried gels through four dominating steps to tranform product. First step, the endothermic peak at 153.7 °C in DSC accounted for 44.78% of the initial weight loss in TG which was assigned to the loss of absorbed or residual water of the gels. Second step, a weight loss stage of about 27.76% in the range of 300–593.5 °C that was accompanied by one manifest

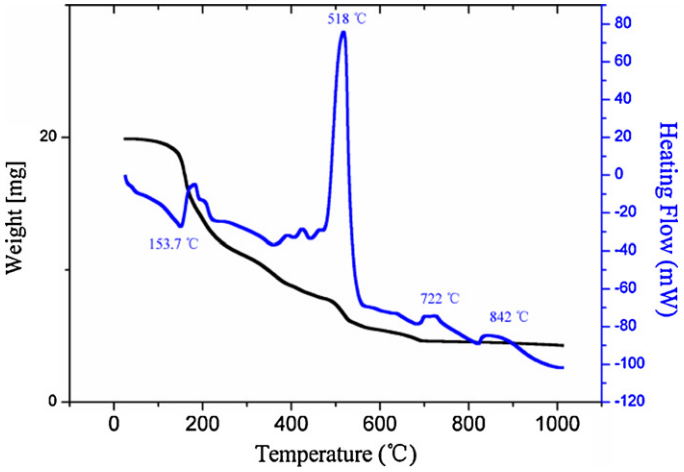

Fig. 1. TG-DTA curves of dried gels for $Ca_2SnO_4:Sm^{3+}$ precursor.

exothermic peak at 518 °C, the exothermic peak at 518 °C was due to the burnout of the organic species. Third step, a weak exothermic peak at 722 °C corresponding to a weight loss of about 5.29%, that was associated with the nucleated crystal phase. Last step, there hardly any weight loss when the temperature beyond 816 °C, and a weak exothermic peak at 842 °C may be assigned to the form of Ca_2SnO_4 crystal phase.

Fig. 2 shows the X-ray diffraction (XRD) patterns of the standard pattern JCPDS No. 74-1493, sample $Ca_2SnO_4:Sm^{3+}$ prepared by solid state reaction and sol–gel method with different mole ratio. When the gel with the molar ratio of Ca:Sn = 2:1, the intermediate phase $CaSnO_3$ appears (Fig. 2b); when the gel with the molar ratio of Ca:Sn = 3:1, the intermediate phase $CaSnO_3$ disappeared, and to form the final product Ca_2SnO_4. The strong peaks of the sample prepared by solid state reaction can be assigned to the phase Ca_2SnO_4. The results suggest that the Ca_2SnO_4 phase can be obtained at lower temperature by sol–gel method.

Ca_2SnO_4 belongs to the Sr_2PbO_4-type structure, with isostructural to that of Sr_2CeO_4 [46,47]. In the structure of Ca_2SnO_4, SnO_6 octahedra are connected in low-dimensional form, SnO_6 octahedra are linked sharing edges with each other and forming

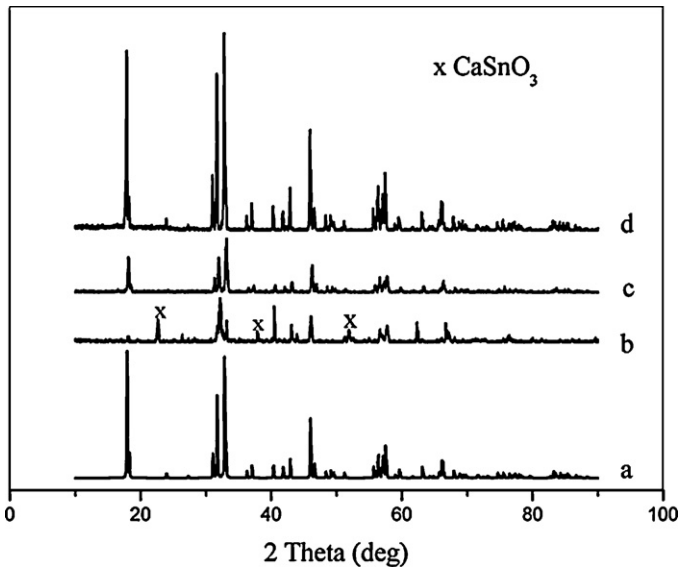

Fig. 2. XRD patterns JCPDS No. 74-1493 database standard for Ca_2SnO_4 (a) and samples $Ca_2SnO_4:Sm^{3+}$ prepared by solid state reaction (d); prepared by sol–gel method with different mole ratio: Ca:Sn = 2:1 (b); Ca:Sn = 3:1 (c).

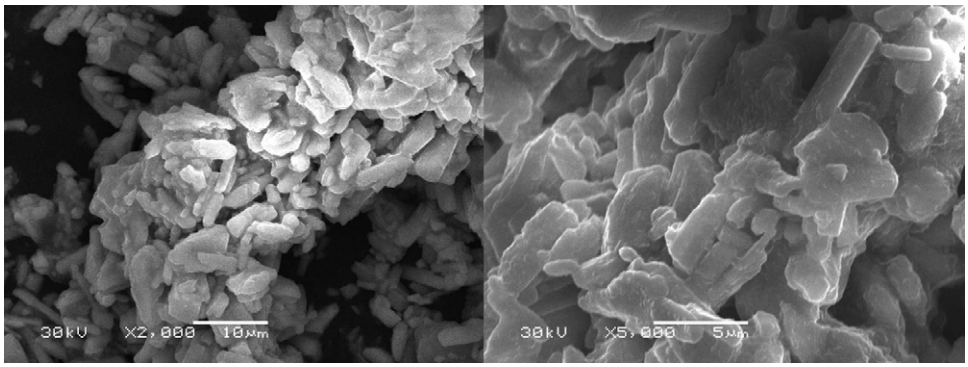

Fig. 3. SEM images of obtained sample Ca_2SnO_4:Sm^{3+} prepared by sol–gel method.

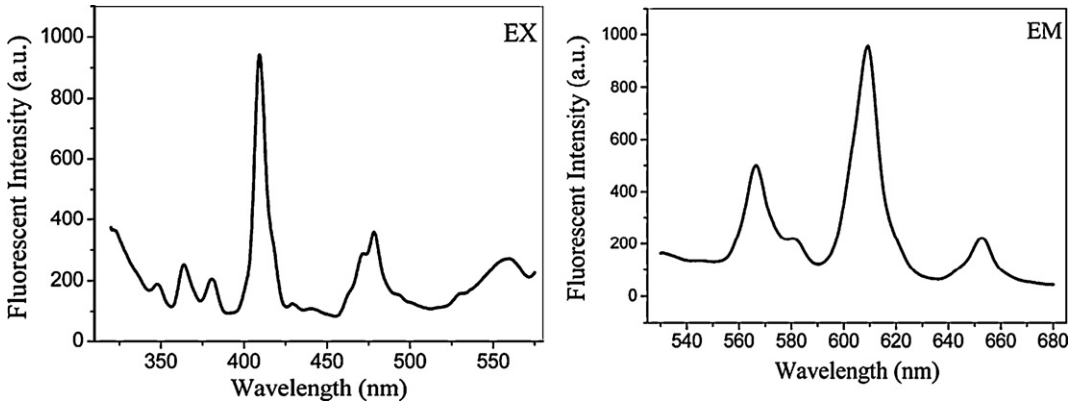

Fig. 4. Typical excitation (λ_{em} = 609 nm) and emission (λ_{ex} = 409 nm) spectra of Ca_2SnO_4:Sm^{3+} prepared by sol–gel method.

one-dimensional chains. Ca^{2+} is seven coordinate and Sn^{4+} is six coordinate [48]. Considering the radius of Ca^{2+} is 1.06 Å (when coordinate number CN = 7) Sm^{3+} 1.02 Å (when coordinate number CN = 7) and Sn^{4+} 0.71 Å (when coordinate number CN = 6), it can be expected that the Sm^{3+} ions occupy the Ca^{2+} sites.

The scanning electron micrograph (SEM) images of sample Ca_2SnO_4:Sm^{3+} prepared by sol–gel method is shown in Fig. 3. Most particles with bar-like shape and a little aggregation were observed in Ca_2SnO_4:Sm^{3+}. The size of the particles reaches about few microns.

The typical excitation and emission spectra of Sm^{3+} doped Ca_2SnO_4 phosphor prepared by sol–gel method are shown in Fig. 4. The excitation spectra consist of a series of peaks in the range of 320–575 nm. The strongest band at 409 nm ($^6H_{5/2} \rightarrow {}^4F_{7/2}$) and some peaks at 348, 364, 381, 409, 470 and 478 nm are ascribed to the transitions from the ground state to the excited states of Sm^{3+}. Under excitation at 409 nm, three strong peaks located at 566, 609 and 653 nm can be assigned to the $^4G_{5/2} \rightarrow {}^6H_J$ (J = 5/2, 7/2, 9/2) transitions of Sm^{3+} ion [31,37,38]. The peak at 609 nm is the strongest one; two peaks exist at 565 and 655 nm, respectively.

From the recorded emission spectra of phosphors Ca_2SnO_4:Sm^{3+} prepared by sol–gel method, the fluorescent intensity depends on the content of Sm^{3+}. The relation between fluorescent intensity and the content of Sm^{3+} is shown in Fig. 5. It was quite clear that the fluorescent intensity increase with the increasing content of Sm^{3+} ion up to 1.5 mol%, then decreased beyond the content due to concentration quenching. The reason lies in that odds of complex of non-radiative transition is increasing as the content of Sm^{3+} is increasing, as a result, the fluorescent intensity of the phosphors become lower.

The luminous colors of the phosphors are reddish orange as result of complex spectra. In general, luminous color is represented

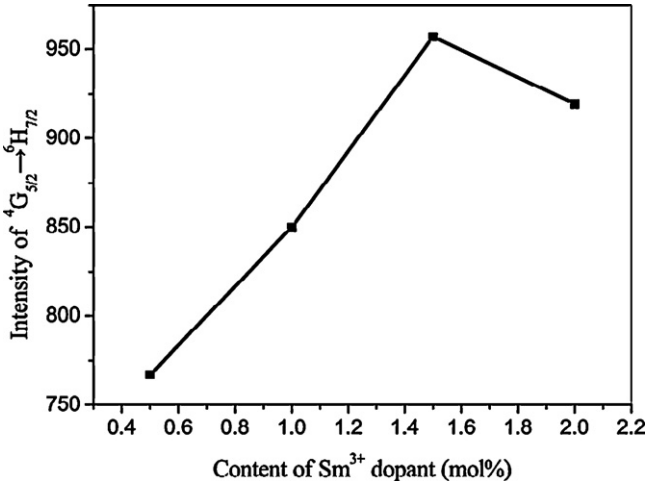

Fig. 5. The relation between fluorescent intensity and the content of Sm^{3+} for the Ca_2SnO_4:Sm^{3+} phosphor prepared by sol–gel method.

by color coordinates and color ratios. The chromaticity coordinates of the phosphor S_3 has been calculated from the spectra using the CIE (Commission International de l'Eclairage, France) system. It has chromaticity coordinates of x = 0.53 and y = 0.47, which locate in the range of reddish orange light emission.

The afterglow decay process for the samples prepared by sol–gel method was studied in the present work. The decay process comprised of a fast and a slow part can be fit by the following equation [49]:

$$I = A_1 \exp\left(\frac{-t}{\tau_1}\right) + A_2 \exp\left(\frac{-t}{\tau_2}\right) + A_3 \exp\left(\frac{-t}{\tau_3}\right) \quad (1)$$

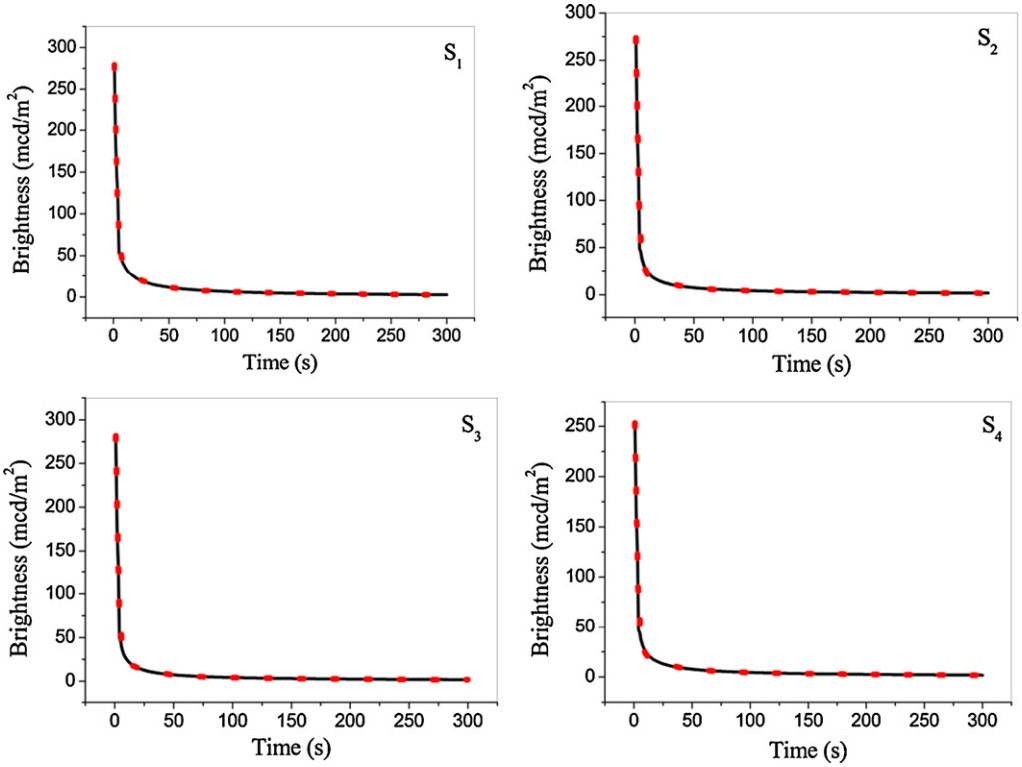

Fig. 6. Afterglow decay curves for $Ca_2SnO_4:Sm^{3+}$ with different contents of Sm^{3+}-doped phosphors prepared by sol–gel method. Red dotted lines show the fitting results. (For interpretation of the references to color in this figure legend, the reader is referred to the web version of the article.)

where I is phosphorescence intensity, A_1, A_2 and A_3 are constants and t is time, τ_1, τ_2 and τ_3 are decay time for exponential components, respectively. All the decay curves of $Ca_2SnO_4:Sm^{3+}$ phosphors are well fitted with triple-exponential components, the results are shown in Fig. 6, and obtained parameters are listed in Table 1.

From Table 1, it can be seen that the constants and decay times are different for samples S_1–S_4. Along with the content increase of Sm^{3+}, the parameters of A_1, A_2, A_3, τ_1, τ_2 and τ_3 also increased, and that reached the biggest when the content of Sm^{3+} increased to 1.5 mol%. After that, the parameters become small. Thus, it is implied that the content of Sm^{3+} in the Ca_2SnO_4 matrix has effects on the afterglow properties. Among them, the sample S_3 has the biggest constants A_1, A_2 and A_3, the longest decay time τ_1, τ_2 and τ_3, which shows the best afterglow characteristic due to the slow decay component. In industry, the afterglow decay time is defined as the duration from the moment of stopping the light excitation to the moment the emission light intensity is reduced to 0.32 mcd/m^2. For sample S_3, the persistent luminescence lasting about 1 h at recognizable intensity level (0.32 mcd/m^2) in dark place, that is to say, the afterglow time of sample S_3 is about 1 h.

The thermoluminescence (TL) spectrum has been a major technique for revealing trapping center. In order to detect trapping properties of $Ca_2SnO_4:Sm^{3+}$ prepared by sol–gel method, the thermoluminescence spectra for samples S_1–S_4 are carried out and shown in Fig. 7. The TL intensity increased as the content of Sm^{3+} was elevated. At a certain content (1.5 mol%), it approached to a maximum, and then decrease as the content of Sm^{3+} increased continuously.

Table 1
Parameters for triple exponential components of $Ca_2SnO_4:Sm^{3+}$ with different contents of Sm^{3+} prepared by sol–gel method.

Sample number	A_1	A_2	A_3	τ_1 (s)	τ_2 (s)	τ_3 (s)
S_1	372.21	31.77	9.04	2.27	25.19	232.40
S_2	425.48	23.87	5.92	1.81	23.09	233.55
S_3	441.49	23.44	5.90	1.80	22.86	245.78
S_4	385.12	22.61	6.25	1.87	23.83	238.91

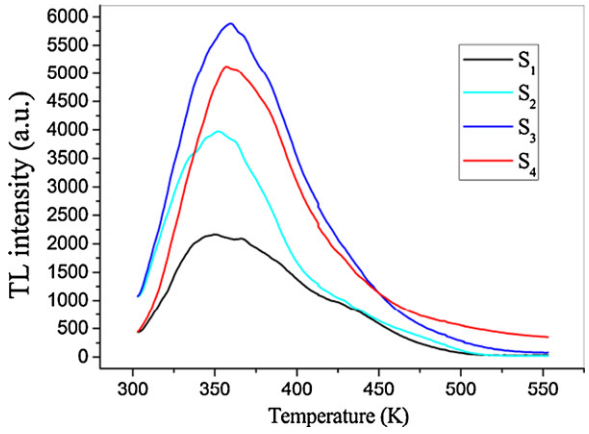

Fig. 7. TL curves for $Ca_2SnO_4:Sm^{3+}$ with different contents of Sm^{3+}-doped phosphors prepared by sol–gel method.

From Fig. 7, it seems that each TL glow curve has a single broad peak without obvious inflection points indicating the presence of other overlapped peaks. However, if we use peak shape method to analyze the parameters, for example, τ, δ, ω and μ_g, defined as: $\omega = \delta + \tau$, $\mu_g = \delta/\omega$, in which ω is the FWHM (full width half maximum), τ is the low-temperature half width, δ is the high-temperature half width and μ_g is the geometrical form factor. The μ_g in the range from 0.53 to 0.67, which seems to be unrealistic since their values lies in between 0.42 and 0.52. The unexpected values of μ_g imply that the broad peaks may consist of more than one peak having closer distribution of their traps depths. So the

Table 2
Estimated E and n_0 from TL spectra for Ca_2SnO_4:Sm^{3+} prepared by sol–gel method.

Sample number	Peak 1 E (eV)	Peak 1 n_0 $(cm^3)^{-1}$	Peak 2 E (eV)	Peak 2 n_0 $(cm^3)^{-1}$
S_1	0.52	3.4×10^4	0.42	3.7×10^4
S_2	0.53	6.7×10^4	0.41	3.7×10^4
S_3	0.52	9.4×10^4	0.43	7.2×10^4
S_4	0.52	9.4×10^4	0.42	6.6×10^4

curve fitting technique was used to analyze the TL curves [41]. The TL curves firstly were done deconvolution based on Gussian function, and then were analyzed the individual deconvoluted peaks using Chen's method by the equation [50]:

$$E = [2.52 + 10.2(\mu_g - 0.42)]\left(\frac{k_B T_m^2}{\omega}\right) - 2k_B T_m \quad (2)$$

$$n_0 = \frac{\omega I_m}{\beta[2.52 + 10.2(\mu_g - 0.42)]} \quad (3)$$

In Eq. (2), k_B is Boltzmann's constant, E is the trap depth; T_m is the temperature of the glow peaks and β is the heating rate (1 K/s for our experiment). In Eq. (3), n_0 is the concentration of trapped charges at $t = 0$, I_m is the TL intensity of the glow peaks. As an instance, the TL curve of sample S_2 and fitting curves are shown in Fig. 8. All the TL curves of Ca_2SnO_4:Sm^{3+} phosphors were fitted successfully by Gussian function, and estimated values of E and n_0 are listed in Table 2.

It can be seen from Table 2 that the values of E for both peaks are very close; the values of E for TL peak 1 are about 0.52 eV, and that for TL peak 2 are about 0.42 eV. It is important for long lasting phosphor to have a suitable energy level (E) within the host. On the one hand, if the energy level is too low, the electron in the trap can return to the energy level of the excited state easily after excitation, thus resulting in short afterglow lifespan. On the other hand, if the energy level is too deep, the thermal energy necessary for the electron return to the excited state level is so difficult to obtain, that the electron cannot return, also resulting in poor afterglow property. It is reported that the trap depths at 0.4–0.6 eV if materials show excellent persistent phosphorescence performance [51,52]. In our work, all samples produced suitable trap depth, which are the origin of the long afterglow phenomenon in this kind of material at room temperature. However, the afterglow characteristics of phosphors with different contents of Sm^{3+}-doped are different; the reason comes from different values of n_0. The parameters n_0 also influence the afterglow characteristics directly. Because n_0 represents the trap concentration, a higher n_0 value (higher trap concentration) will produce a higher initial luminescence obviously, since a large amount of traps will capture more free electrons generated by the UV illumination. From Table 2, it is obvious that the values of n_0 for TL peak 1 increase with the increasing content of Sm^{3+} ion up to 1.5 mol%, then remain the same values beyond the content; for TL peak 2, samples S_1 and S_2 have identical values, sample S_3 has the biggest n_0, and leads to the best afterglow characteristics.

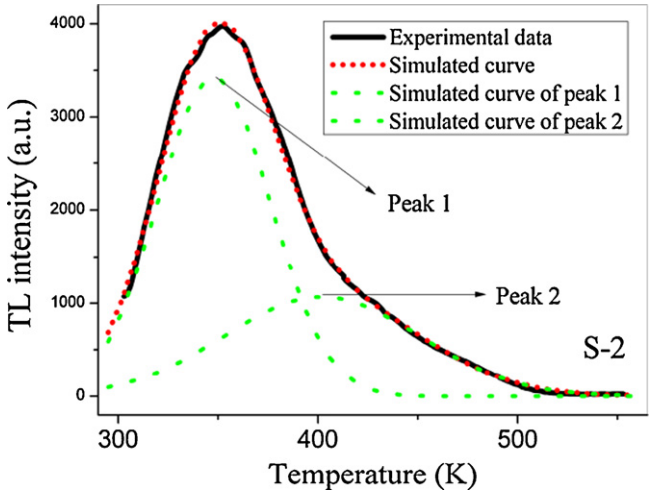

Fig. 8. TL curve of sample S_2, solid line is the measured curve; the dotted lines are the synthesized Gussian curves.

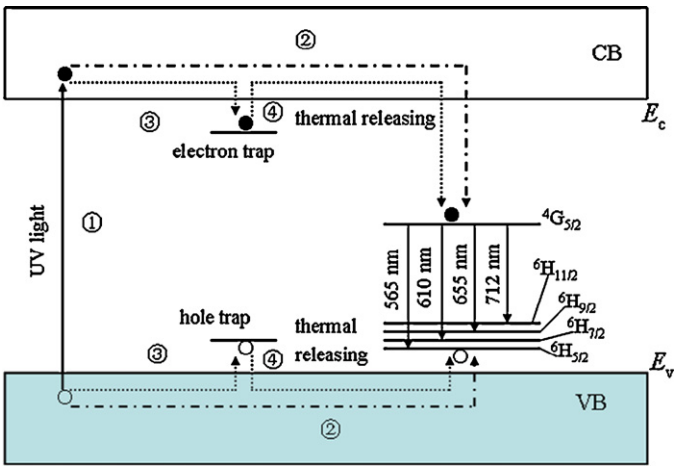

Fig. 9. The schematic graph of phosphorescence mechanism for Ca_2SnO_4:Sm^{3+}. ● represent electron; ○ represent hole.

On the basis of above analysis and discussion, we are trying to explain phosphorescence mechanism of Ca_2SnO_4:Sm^{3+}. In the Ca_2SnO_4:Sm^{3+} phosphor, Sm^{3+} is incorporated on Ca^{2+} sites. The substitution of Sm^{3+} ion for Ca^{2+} is non-equivalent substitution, and it can be taken place according to the equation:

$$Sm_{Ca} \leftrightarrow Sm_{Ca}^{\bullet} + e' \quad (4)$$

In theory, there are two possible pathways of charge compensation to keep the charge balance. One pathway is electronic compensation. In these samples, the element Sn is considered as a multivalent ion [53]. Thus, there is a possibility that some of the Sn^{4+} ions captured electrons liberated in Eq. (4) and change their valence state to Sn^{2+} and Sn^{3+}. Sn^{2+} and Sn^{3+} at the Sn^{4+} ion sites will come into being structure defects, and they can be treated as sites for localization of charge carries (electrons) and play the role of hole traps. The other possible pathway of charge compensation is vacancy compensation, the vacancies of metal ions generated in the crystal lattice to compensate charge. Two Sm^{3+} ions replace three Ca^{2+} ions, which create two $Sm_{Ca}^{\bullet}$ positive defects and one V''_{Ca} (vacancy) negative defect. The equation of defects is expressed as follows:

$$3Ca^{2+} + 2Sm^{3+} \rightarrow V''_{Ca} + 2Sm_{Ca}^{\bullet} \quad (5)$$

The structure defects Sn^{3+} and Sn^{2+}, the defects V''_{Ca} may act as hole trapping centers [54,55], while the defects $Sm_{Ca}^{\bullet}$ may act as electron trapping centers. In Sm^{3+}-doped samples, Sm^{3+} is not only the provider of traps but also the activator itself. The schematic graph of phosphorescence mechanism for Ca_2SnO_4:Sm^{3+} is shown in Fig. 9. After irradiation with the ultraviolet light (process numbered ①), most of the excitation energy of related to the excited carries (electrons or holes) will be transferred through the host directly to the luminescence centers Sm^{3+}, followed by the characteristic emissions of Sm^{3+} as the luminescence (process numbered ②). However, the trapping centers capture some of the excited carriers and stored part of the excitation energy (process numbered ③), in place of returning to the ground states. Subsequently, the

carriers will be released from the trapping centers under the action of thermal activation at proper temperature, and transferred via the host to the Sm^{3+} ions, (process numbered ④), followed by recombine and resulting the characteristic emissions of Sm^{3+} as long afterglow phosphorescence since the carries transferred from the trap has a slow released ratio.

4. Conclusions

In summary, a reddish orange long afterglow phosphor $Ca_2SnO_4:Sm^{3+}$ was successfully prepared by sol–gel method at lower temperature. The influences of content of Sm^{3+} on PL, afterglow decay curves and TL properties have been studied. The results of fitting the experimental data of decay curves revealed that Sm^{3+}-doped Ca_2SnO_4 phosphor in terms of triple-exponential decay model. The afterglow time is about 1 h. The results of fitting TL glow curves show there are two peaks with suitable trap depths in the phosphor, which create the persistent phosphorescence of Sm^{3+} characteristic luminescence. The defects V''_{Ca}, structure defects Sn^{3+} and Sn^{2+} may act as hole trapping centers, while the defects $Sm_{Ca}^{\bullet}$ may act as electron trapping centers, and trapping centers play an essential role for photo energy storage in persistent phosphors.

Acknowledgements

The authors thank the National Natural Science Foundation of China (20771048, 20931003, J0730425), the Fundamental Research Funds for the Central Universities (lzujbky-2009-k06) and Natural Science Foundation of Gan Su Province (0710RJZA041) for financial support.

References

[1] F.C. Palilla, A.K. Levine, R.T. Majia, J. Electrochem. Soc. 115 (1968) 642–644.
[2] T. Matsuzawa, Y. Aoki, N. Takeuchi, Y. Murayama, J. Electrochem. Soc. 143 (1996) 2670–2673.
[3] J.T. Piegza, J. Niittykoski, J. Hölsä, E. Zych, Chem. Mater. 20 (2008) 2252–2261.
[4] M. Kowatari, D. Koyama, Y. Satoh, K. Iinuma, S. Uchida, Nucl. Instrum. Meth. Phys. Res. A 480 (2002) 431–439.
[5] J.R. Qiu, K. Miura, H. Inouye, Y. Kondo, T. Mitsuyu, K. Hirao, Appl. Phys. Lett. 73 (1998) 1763–1765.
[6] C.Y. Li, Y.N. Yu, S.B. Wang, Q. Su, J. Non-Crystal. Solids 321 (2003) 191–196.
[7] J.R. Qiu, M. Kawasaki, K. Tanaka, Y. Shimizugawa, K. Hirao, J. Phys. Chem. Solids 59 (1998) 1521–1525.
[8] Z.X. Yuan, C.K. Chang, D.L. Mao, W.J. Ying, J. Alloys Compd. 377 (2004) 268–271.
[9] B. Liu, C.S. Shi, M. Yin, L. Dong, Z.G. Xiao, J. Alloys Compd. 387 (2005) 65–69.
[10] X.M. Teng, W.D. Zhuang, Y.S. Hu, C.L. Zhao, H.Q. He, X.W. Huang, J. Alloys Compd. 458 (2008) 446–449.
[11] C. Liu, Y.H. Wang, Y.H. Hu, R. Chen, F. Liao, J. Alloys Compd. 470 (2009) 473–476.
[12] B.F. Lei, Y.L. Liu, J.W. Zhang, J.X. Meng, S.Q. Man, S.Z. Tan, J. Alloys Compd. 495 (2010) 247–253.
[13] S.X. Lian, Y. Qi, C.Y. Rong, L.P. Yu, A.L. Zhu, D.L. Yin, S.B. Liu, J. Phys. Chem. C 114 (2010) 7196–7204.
[14] A. Lecointre, A. Bessirère, A.J.J. Bos, P. Dorenbos, B. Viana, S. Jacquart, J. Phys. Chem. C 115 (2011) 4217–4227.
[15] W.Y. Li, Y.L. Liu, P.F. Ai, Mater. Chem. Phys. 119 (2010) 52–56.
[16] P. Huang, C.E. Cui, S. Wang, Opt. Mater. 32 (2009) 184–189.
[17] J. Llanos, R. Castillo, D. Espinoza, R. Olivares, I. Brito, J. Alloys Compd. 509 (2011) 5295–5299.
[18] A. Katelnikovas, J. Jurkevičius, K. Kazlauskas, P. Vitta, T. Jüstel, A. Kareiva, A. Žukauskas, G. Tamulaitis, J. Alloys Compd. 509 (2011) 6247–6251.
[19] R. Praveena, L. Shi, K.H. Jang, V. Venkatramu, C.K. Jayasankar, H.J. Seo, J. Alloys Compd. 509 (2011) 859–863.
[20] Y. Dong, Z.S. Wu, X.L. Han, R. Chen, W.J. Gu, J. Alloys Compd. 509 (2011) 3638–3643.
[21] B.C. Cheng, L.T. Fang, Z.D. Zhang, Y.H. Xiao, S.J. Lei, J. Phys. Chem. C 115 (2011) 1708–1713.
[22] D.B. Bem, H.C. Swart, A.S. Luyt, F.B. Dejene, J. Appl. Polym. Sci. 121 (2011) 243–252.
[23] D.B. Bem, H.C. Swart, A.S. Luyt, M.M. Duvenhage, F.B. Dejene, Polym. Compos. 32 (2011) 219–226.
[24] S.S. Yao, Y.Y. Li, L.H. Xue, Y.W. Yan, J. Alloys Compd. 490 (2010) 200–203.
[25] S.S. Yao, L.H. Xue, Y.W. Yan, J. Alloys Compd. 509 (2011) 1870–1873.
[26] P. Zhang, L.X. Li, M.X. Xu, L. Liu, J. Alloys Compd. 456 (2008) 216–219.
[27] Y.J. Huang, H.P. You, Y.H. Song, G. Jia, M. Yang, Y.H. Zheng, L.H. Zhang, K. Liu, J. Cryst. Growth 312 (2010) 3214–3218.
[28] P.C. de, S. Filho, O.A. Serra, J. Phys. Chem. C 115 (2011) 636–646.
[29] Y.F. Xu, D.K. Ma, M.L. Guan, X.A. Chen, Q.Q. Pan, S.M. Huang, J. Alloys Compd. 502 (2010) 38–42.
[30] F. He, P.P. Yang, D. Wang, C.X. Li, N. Niu, S.L. Gai, M.L. Zhang, Langmuir 27 (2011) 5616–5623.
[31] E.L. Cates, M. Cho, J.H. Kim, Environ. Sci. Technol. 45 (2011) 3680–3686.
[32] J.H. Kim, K.Y. Jung, J. Lumin. 131 (2011) 1487–1491.
[33] X.H. Tan, J. Alloys Compd. 477 (2009) 648–651.
[34] Y.S. Chang, Z.R. Shi, Y.Y. Tsai, S. Wu, H.L. Chen, Opt. Mater. 33 (2011) 375–380.
[35] C.F. Guo, J. Yu, J.H. Jeong, Z.Y. Ren, J.T. Bai, Physica B 406 (2011) 916–920.
[36] Y.C. Chen, Y.H. Chang, B.S. Tsai, Opt. Mater. 27 (2005) 1874–1878.
[37] X. Lin, X.S. Qiao, X.P. Fan, Solid State Sci. 13 (2011) 579–583.
[38] Z.H. Xu, X.J. Kang, C.X. Li, Z.Y. Hou, C.M. Zhang, D.M. Yang, G.G. Li, J. Lin, Inorg. Chem. 49 (2010) 6706–6715.
[39] G. Lakshminarayana, R. Yang, M.F. Mao, J.R. Qiu, I.V. Kityk, J. Non-Cryst. Solids 355 (2009) 2668–2673.
[40] G. Lakshminarayana, R. Yang, M.F. Mao, J.R. Qiu, G.A. Kumar, I.V. Kityk, J. Phys. D: Appl. Phys. 42 (2009) 015414.
[41] A. Lempicki, J. Glodo, Nucl. Instrum. Methods Phys. Res. A 416 (1998) 333–344.
[42] D.D. Jia, J. Zhu, B.Q. Wu, J. Electrochem. Soc. 147 (2000) 386–389.
[43] C.B. Liu, G.B. Che, Z.L. Xu, Q.W. Wang, J. Alloys Compd. 474 (2009) 250–253.
[44] H.Y. Wu, Y.H. Hu, Y.H. Wang, C.J. Fu, Mater. Sci. Eng. B 172 (2010) 276–282.
[45] H.Y. Wu, Y.H. Hu, L. Chen, X.J. Wang, J. Alloys Compd. 509 (2011) 4304–4307.
[46] E. Danielson, M. Devenney, D.M. Giaquinta, J.H. Golden, R.C. Haushalter, E.W. McFarland, D.M. Poojary, C.M. Reaves, W.H. Weinberg, X.D. Wu, J. Mol. Struct. 470 (1998) 229–235.
[47] E. Danielson, M. Devenney, D.M. Giaquinta, J.H. Golden, R.C. Haushalter, E.W. McFarland, D.M. Poojary, C.M. Reaves, W.H. Weinberg, X.D. Wu, Science 279 (1998) 837–839.
[48] H.M. Yang, J.X. Shi, M.L. Gong, J. Solid State Chem. 178 (2005) 917–920.
[49] T. Katsumata, T. Nabae, K. Sasajima, S. Komuro, T. Morikawa, J. Electrochem. Soc. 144 (1997) L243–L245.
[50] R. Chen, J. Electrochem. Soc. 116 (1969) 1254–1257.
[51] R. Sakai, T. Katsumata, S. Komuro, T. Morikawa, J. Lumin. 85 (1999) 149–154.
[52] J.Y. Kuang, Y.L. Liu, J. Electrochem. Soc. 153 (2006) G245–G247.
[53] S. Upadhyay, O. Parkash, D. Kumar, J. Phys. D: Appl. Phys. 37 (2004) 1483.
[54] Y.H. Chen, X.R. Cheng, M. Liu, Z.M. Qi, C.S. Shi, J. Lumin. 129 (2009) 531–535.
[55] F. Clabau, X. Rocquefelte, T. Le Mercier, P. Deniard, S. Jobic, M.-H. Whangbo, Chem. Mater. 18 (2006) 3212–3220.